Modelling of the kinetic transition in zirconium based alloys: Application to the oxidation of Zircaloy-4 by water vapour

Marc Tupin, Françoise Valdivieso, Michèle Pijolat, Michel Soustelle, Alain Frichet, Pierre Barberis

Modelling of the kinetic transition in zirconium based alloys: Application to the oxidation of Zircaloy-4 by water vapour

MARC TUPIN(1), FRANÇOISE VALDIVIESO(1), MICHELE PIJOLAT(1*), MICHEL SOUSTELLE(1), ALAIN FRICHET(2), PIERRE BARBERIS(3).

(1) *Ecole Nationale Supérieure des Mines, Centre SPIN, Département ProcESS, LPMG, UMR CNRS 5148, 158 Cours Fauriel, 42023 SAINT-ETIENNE, Cedex 2, France*
(2) *FRAMATOME-ANP, 10 rue Juliette Récamier, 69456 LYON, Cedex 06, France.*
(3) *CEZUS, Centre de Recherches, 73043 Ugine cedex, France.*
(3) *mpijolat@emse.fr*

Keywords:
zirconium alloys ; oxidation kinetics ; transition ; oxide layer damage

Abstract.

The kinetic curves of oxidation of Zircaloy-4 exhibit a transition, which is a sharp increase in the oxidation rate when the oxide thickness reaches a critical value. The pre-transition stage is controlled by the diffusion of oxygen vacancies in the oxide layer. In the post-transition stage, oxygen or water vapour have an accelerating effect on the oxidation (whereas they have no influence during the pre-transition) and the oxide layer is damaged, with large cracks parallel to the metal/oxide interface and connected to the gaseous atmosphere by pores. Consequently, it is clear that the post-transition stage cannot be accounted for by the same mechanism as in pre-transition. In this paper, we propose a geometrical modelling allowing to describe the progressive transformation of the oxide layer during the transition. This model is based on a random appearance of pores (connected to the external surface) which leads to the transformation, from a pre-transition stage to the post-transition stage, of small sections s_0 of the oxide layer (analogy with the models of thermal transformations of powders, involving the processes of nucleation and growth of a new phase). The model allows to describe the kinetic curves obtained for the oxidation by water vapour of Zircaloy-4.

Introduction

In a previous work [1], we have studied the oxidation kinetics of Zircaloy-4 by water vapour, between 500 and 530°C, under controlled partial pressure of water vapour (13 to 73hPa) and hydrogen (10hPa). The oxidation curves exhibit two kinetic stages, separated by a transition.

Although the oxidation is not strictly parabolic, it has been shown that the pre-transition stage is controlled by the diffusion of oxygen vacancies in the oxide layer, as usually suggested in the literature data [2-6]. The sub-parabolic curves could be well fitted with the following law:

$$\frac{dX}{dt} = \frac{k_1}{X}\exp\left(-k_2 X\right) \qquad (1)$$

in which X is the oxide thickness, k_1 and k_2 are constants which meaning depends on the physical modelling leading to Eq. (1) [6-8]. This law can be obtained either considering the existence of barriers for the diffusing species (k_2 : number of barriers per unit of length) or the effect of a gradient of compressive stresses in the oxide layer.

In the post-transition stage, water vapour pressure has an accelerating effect on the oxidation rate [1, 2, 9, 10] (whereas it has no influence during the pre-transition [1, 2, 9]) and

the oxide layer is damaged [1, 2, 9], with large cracks parallel to the metal/oxide interface and connected to the gaseous atmosphere by pores. Consequently, it is clear that the post-transition stage cannot be accounted for by the same mechanism as in pre-transition.

In this paper, a modelling of the transition is described, taking into account the degradation of the oxide layer.

Experimental results

Experimental.

A 0.4 mm thick sheet of recrystallised Zircaloy-4 alloy was provided by Cezus, and samples were cut to 10 x 10 mm for thermogravimetric experiments. The alloy composition is indicated in Table 1. The sample surface was cleaned with an equimolar solution of ethanol and acetone in ultrasonic waves, then with pure ethanol and dried with compressed air.

C [ppm]	Cr [ppm]	Fe [ppm]	Hf [ppm]	N [ppm]	O_2 [ppm]	Si [ppm]	Sn (%)
106	1075	2203	46	35	1260	35	1.46

Table 1: Composition of the Zircaloy-4 alloy

The oxidation curves were obtained in isothermal and isobaric conditions at 500 and 530°C with a symmetrical thermoanalyser SETARAM TAG16, under a flowing mixture of water vapour and hydrogen in helium. The flowrates of the gases were controlled by mass-flowmeters (Brooks 5850S), the total flowrate being 2.3 $l.h^{-1}$, and the partial pressure of hydrogen being usually equal to 10 hPa. The water vapour partial pressure was in the range 13-80 hPa, and was maintained at the chosen value by a thermoregulated bath. It was controlled using humidity sensors (Transmicor 241-242 Coreci), placed at the inlet and outlet of the furnace.

The morphology of the oxide layers was observed by scanning electron microscopy (SEM DSM 960A Zeiss).

Shape of the kinetic curves.

Fig. 1 represents kinetic curves giving the mass gain m(t) versus time, and its derivative (dm/dt), obtained at 530°C (after an initial temperature rise of 30°C/min from room temperature to 530°C), under 10 hPa in hydrogen and either 13 hPa or 73 hPa in water vapour.

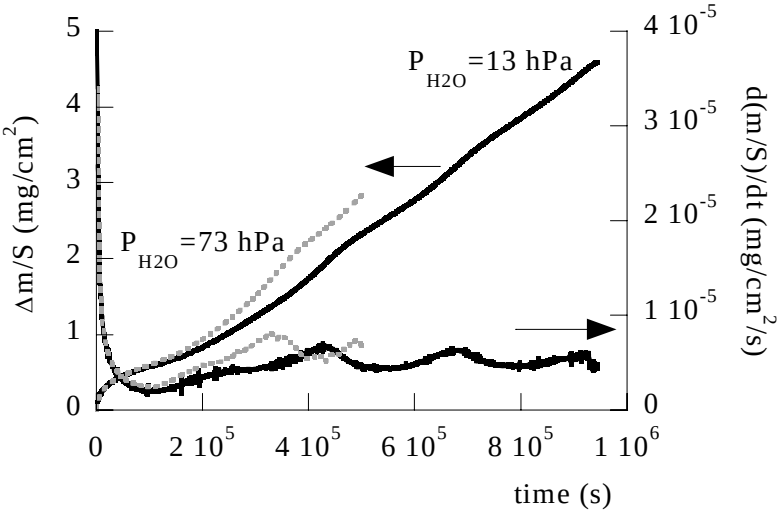

Figure 1: Weight gain and its derivative versus time for Zircaloy-4 at 530°C (10 hPa hydrogen) : 13 hPa (—) and 73 hPa (---) water vapour.

Before the transition, the rate decreases continuously, the minimum of the rate corresponding to an oxide thickness (calculated from the weight gain) of about 4 µm. After the transition, the curves present successive periods of increasing and decreasing rate.

It can be noticed that the water vapour pressure has no effect on the oxidation rate before the transition, but it has an accelerating influence in the post-transition stage. This observation was confirmed using jumps in water vapour pressure [1]. In pre-transition, these results are in agreement with the diffusion of oxygen vacancies as a controlling step.

Characterisation of the samples.

The cross-sectional views of the oxide scale grown during the pre-transition region present a continuous and uniform layer adherent to the substrate. Fig. 2a shows a micrograph obtained with a sample oxidised during 4 hours at 530°C in 13 and 10 hPa of water vapour and hydrogen, respectively. The layer thickness calculated from the weight gain is 1.7 µm. No cracks connected to the gaseous atmosphere could be observed; the interface is more or less regularly undulated. Short cracks parallel to the interface appear regularly inside the layer.

Similar cracks exist in the samples obtained after the kinetic transition (Fig. 2b and 2c), but their number has increased a lot. Moreover, their coalescence has probably formed the large parallel cracks located at various depths under the surface (3.5 µm in Fig. 2b, 20 µm in Fig. 2c). Some large cracks perpendicular to the interface are also observed [11].

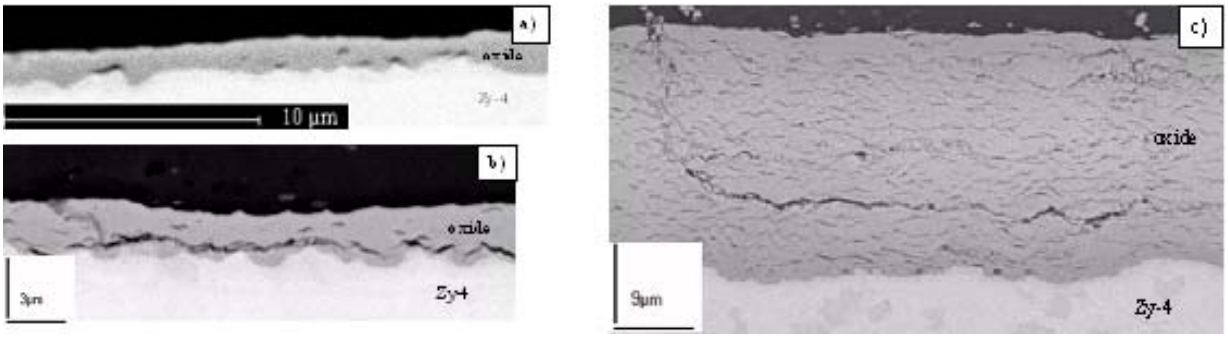

Figure 2: Cross sectional views of Zircaloy-4 samples oxidised at 530°C (P_{H2O}=13hPa, P_{H2}=10hPa) ; in pre- (a) and post-transition stages (b and c).

From these results, it appears that a new mechanism must be considered to account for the kinetic transition, taking into account the partial pressure effects and the degradation of the oxide layer.

Modelling of the kinetic transition.

Principles of the modelling.

Assuming that the transition does not occur at the same time on the whole oxide layer, it can be considered that the layer consists in two kinds of co-existing regions : those already in the post-transition stage, and those still in the pre-transition stage. Consequently, the oxidation rate (followed for example by gravimetry) is the sum of two terms, one corresponding to the growth of zones which are in the pre-transition stage and the other representing the contribution of the post-transition zones. We propose a geometrical modelling in order to describe the progressive transformation of the oxide layer during the transition.

The principle of the modelling is based on the models developed for thermal transformations of powders, involving the competition between the nucleation of the new phase and the growth of the nuclei [12]. In our case, the model is based on a random connection of pores to the external surface (analogy with nuclei), which leads to the transformation, from a pre-transition stage to the post-transition stage, of small sections s_0 of the oxide layer. The evolution of the surface of the oxide layer during the transition is schematically represented on Fig. 3.

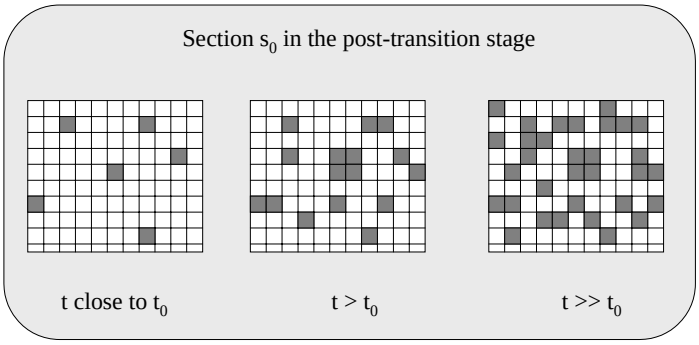

Figure 3: Schematic representation of the surface evolution of the oxide layer during the transition (t_0 is the transition time).

The frequency of apparition of sections s_0 is denoted γ (number.m^{-2}.s^{-1}). Three laws of variations of γ with time have been considered: $\gamma_0(t-t_0)^n$, in which t_0 is the transition time [13] and n can take the values 0, 1 or 2.

During the time $d\tau$, the variation of the number of sections s_0 on the surface $S_L(\tau)$ which is still in the pre-transition stage is:

$$(*)\ dN = \gamma\, S_L(\tau)\, d\tau \qquad (2)$$

The surface $S_L(\tau)$ being the product of s_0 by the number of sections (N) still in the pre-transition stage, it comes :

$$(*)\ dN = \gamma\, s_0\, N(\tau)\, d\tau \qquad (3)$$

Integration of Eq. 3 between the beginning of the transition (t_0) and t leads to:

$$N(t) = N_0 \exp\left(-\frac{s_0\gamma_0(t-t_0)^{n+1}}{n+1}\right) \qquad (4)$$

where N_0 is the number of sections s_0 at time t_0. For all the sections s_0 passing in the post-transition stage at time τ, it is assumed that a step of the oxidation mechanism is rate-controlling. Thus, the oxidation rate dX/dt due to the sections being in post-transition stage at time t is:

$$\frac{dX}{dt} = \frac{V_e n_0}{s_0 N_0}\Phi_{post}\int_{t_0}^{t} E_{post}(t,\tau)\gamma s_0 N_0 \exp\left(-\frac{\gamma_0 s_0}{n+1}(\tau-t_0)^{n+1}\right)d\tau \qquad (5)$$

where Φ_{post} is the surface growth rate (mol.s^{-1}.m^{-2}) and E_{post} (in m^2.mol^{-1}) is representative of the dimensions of the reaction area where the rate-controlling step is located. V_e and n_0 are respectively the molar volume of the oxide and the initial amount in metal.

It must be added to this rate the contribution of the sections s_0 which are still in the pre-transition stage, which leads to the expression of the oxidation rate:

$$\frac{dX}{dt} = \frac{V_e\, n_0}{s_0\, N_0}\left\{\begin{array}{l}\Phi_{post}\int_{t_0}^{t} E_{post}(t,\tau)\,\gamma_0\,(\tau\text{-}t_0)^n\, s_0\, N_0 \exp\left(-\frac{\gamma_0\, s_0}{n+1}(\tau\text{-}t_0)^{n+1}\right)d\tau \\ +\Phi_{pre}\, E_{pre}(t,\tau)\, N_0 \exp\left(-\frac{\gamma_0\, s_0}{n+1}(t\text{-}t_0)^{n+1}\right)\end{array}\right\} \qquad (6)$$

where Φ_{pre} (mol.s^{-1}.m^{-2}) and E_{pre} (m^2.mol^{-1}) represent the surface growth rate and the dimensions of the reaction area relative to the rate-limiting step of the pre-transition stage.

As an example, we can write the expressions of the oxidation rate when the pre-transition stage is controlled by a diffusion step, and the post-transition stage by either an interface step (Eq. 7) or a diffusion step (Eq. 8):

$$\frac{dX}{dt} = \frac{V_e}{N_0}\left\{ \Phi_{post\_interface} \int_{t_O}^{t} \gamma_0 (\tau - t_0)^n s_0 N_0 \exp\left(-\frac{\gamma_0 s_0}{n+1}(\tau - t_0)^{n+1} \right) d\tau + N_0 X_0 \Phi_{pré} \frac{\exp\left(-\frac{\gamma_0 s_0}{n+1}(t - t_0)^{n+1} \right)}{X(t)} \right\} \quad (7)$$

$$\frac{dX}{dt} = V_e X_0 \left\{ \frac{\Phi_{post\_diffusion}}{N_0} \int_{t_O}^{t} \frac{\gamma_0 (\tau - t_0)^n s_0 N_0 \exp\left(-\frac{\gamma_0 s_0}{n+1}(\tau - t_0)^{n+1} \right) d\tau}{\left(X(t) - X(\tau) \right)} + \Phi_{pré} \frac{\exp\left(-\frac{\gamma_0 s_0}{n+1}(t - t_0)^{n+1} \right)}{X(t)} \right\} \quad (8)$$

Fig. 4 shows the shape of the rate curves obtained in these two cases (the law of variation of the frequency of apparition of sections s_0, γ, being $\gamma_0(t\text{-}t_0)^2$).

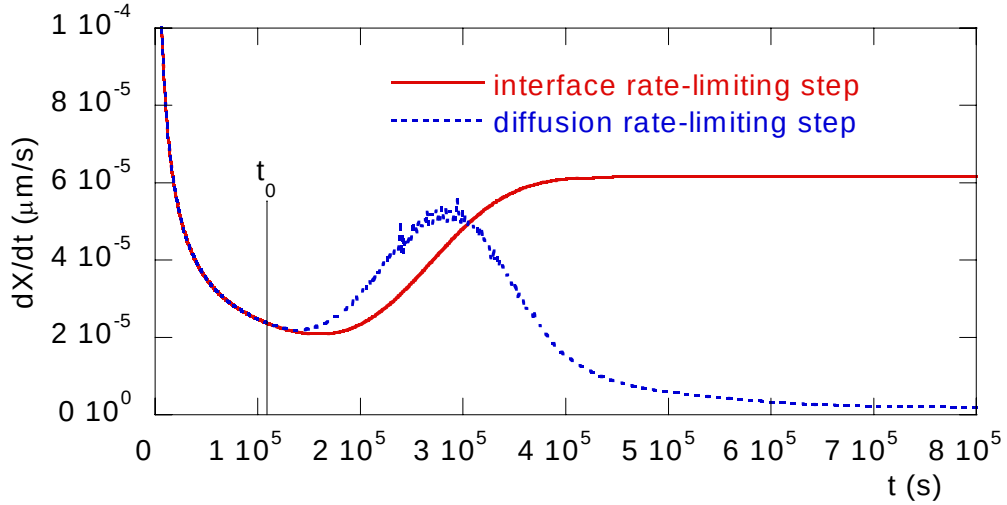

Figure 4: Oxidation rate dX/dt versus time calculated using Eq. (7) (interface rate-limiting step in post-transition (—)) or Eq. (8) (diffusion rate-limiting step in post-transition (---)).

If in the post-transition stage a mixed reaction-diffusion process is rate-controlling, the oxidation rate is given in most cases [13] by:

$$\frac{dX}{dt} = V_e \left\{ \Phi_{d_2} \frac{\Phi_i}{N_0} \int_{t_O}^{t} \frac{\gamma_0 (\tau - t0)^n s_0 N_0 \exp\left(-\frac{\gamma_0 s_0}{n+1} (\tau - t_0)^{n+1} \right) d\tau}{\Phi_{d_2} + \frac{\Phi_i}{X_0} \left(X(t) - X(\tau) \right)} + X_0 \Phi_{d_1} \frac{\exp\left(-\frac{\gamma_0 s_0}{n+1} (\tau - t_0)^{n+1} \right)}{X(t)} \right\} \quad (9)$$

in which Φ_i is the rate of the interface step if it was rate-controlling, and Φ_{d2} the rate of the diffusion step if it was rate-controlling ; Φ_{d1} is the rate of the diffusion step considered as rate-limiting in the pre-transition stage. Fig. 5 represents kinetic curves calculated using Eq. 9, for various values of the ratio Q equal to $Q = \Phi_i / X_0 \Phi_{d_2}$:

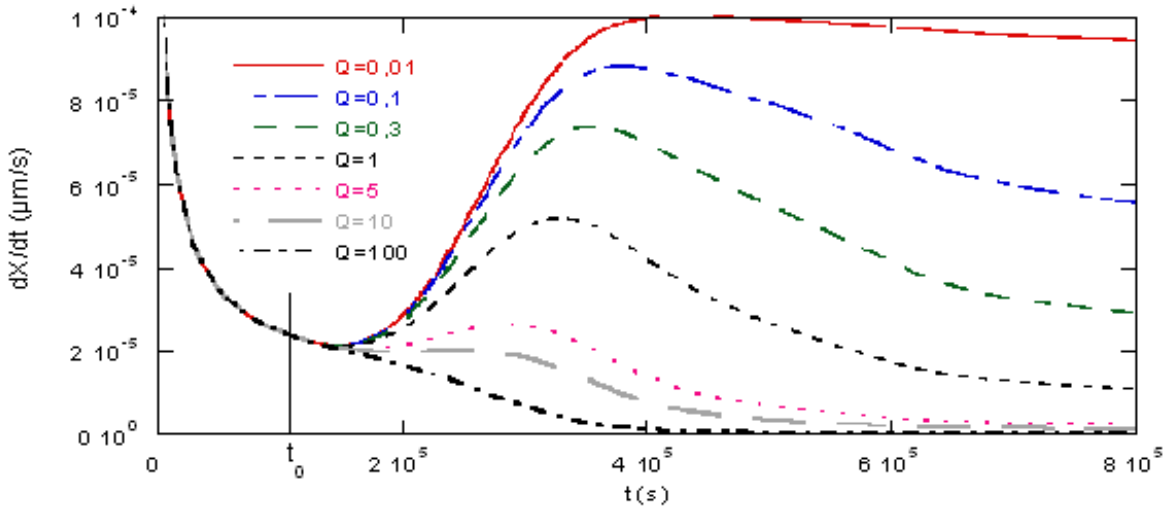

Figure 5: Curves simulated using Eq. 9, for various values of the ratio Q of the rates of the interface and diffusion steps.

Application to the oxidation of Zircaloy-4 by water vapour.

This model has been used to account for the oxidation kinetics of Zircaloy-4 by water vapour. A curve representing the rate dX/dt versus the oxide thickness X is given in Fig. 6 (T=530°C, P_{H2O} =13 hPa, P_{H2} = 10 hPa): the rate decreases in pre-transition, up to a thickness of about 3 µm, then it increases and reaches a value approximately constant between 3 and 8 µm, finally it increases again and passes through a maximum between 8 and 16 µm.

In the pre-transition stage, the oxidation rate is described by Eq. 1.

In the post-transition stage, between 3 and 8 µm, the shape of the curve can be accounted for by an interface rate-limiting step according to Eq. 10 (which is deduced from Eq. 7, taking into account the term $\exp(-k_2 X)$ in the pre-transition diffusion rate) :

$$\frac{dX}{dt} = V_e \left\{ \frac{\Phi_{post}}{N_0} \int_{t_0}^{t} \gamma_0 (\tau - t_0)^2 s_0 N_0 \exp\left(-\frac{\gamma_0 s_0}{3} (\tau - t_0)^3 \right) d\tau + X_0 \Phi_{d_1} \frac{\exp\left(-\frac{\gamma_0 s_0}{3} (t - t_0)^3 \right)}{X(t) - X_a} \exp\left(-k_2 \left(X(t) - X_a \right) \right) \right\} \quad (10)$$

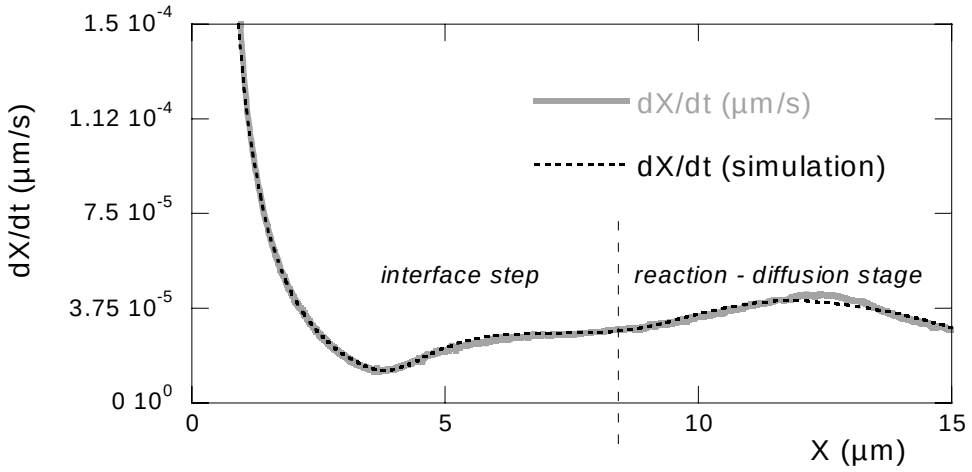

Figure 6: Oxidation rate dX/dt versus the oxide thickness X ; experimental curve (continuous line) and simulated curve using Eq. 10 and 11 (dotted line).

It is in agreement with the formation of porosity connected to the gaseous atmosphere: we can imagine that in some places in the oxide layer, the gas has a direct access to a very small dense oxide layer (through pores and cracks), in which the diffusion is no more rate-limiting, an interface step becoming rate-controlling then. This assumption could also account for the influence of the partial pressure of water vapour observed in the post-transition stage (which can not be accounted for considering only a diffusion rate-limiting step).

Nevertheless, this equation does not allow to interpret the increase of the oxidation rate for X>8µm. Thus, in the range [8 –16 µm], we can assume a mixed reaction-diffusion stage, due to the fact that the thickness of the dense oxide layer increases again. Thus, Eq. 11 (deduced from Eq. 9) is obtained:

$$\frac{dX}{dt} = V_e \left\{ \frac{\Phi_{i_2}}{N_0} \int_{t_1}^{t} \frac{\gamma'_0 (\tau - t_1)^2 s_0 N_0 \exp\left(-\frac{\gamma'_0 s_0}{3} (\tau - t_1)^3 \right)}{1 + \frac{\Phi_{i_2}}{\Phi_{d2}} \frac{\left(X(t) - X(\tau) \right)}{X_0}} d\tau + X_0 \Phi_{post} \exp\left(-\frac{\gamma'_0 s_0}{3} (t - t_1)^3 \right) \right\} \quad (11)$$

in which Φ_{post}, Φ_{i2}, Φ_{d2} are respectively the rate of the interface rate-controlling step for 3 < X <8µm, and the rates of the interface and diffusion steps involved in the mixed reaction-diffusion stage (8 < X < 16µm) ; t_1 is the time corresponding to X = 8µm.

In Fig. 6, the dotted line corresponds to a curve calculated using Eq. 10 (for 3 < X <8 µm, interface rate-limiting step) and 11 (for 8 < X <16 µm, reaction-diffusion stage), the values of the various parameters being indicated in table 2. This calculated curve is in a very good agreement with the experimental one.

Φ_{d1} [mol.m^{-2}.s^{-1}]	X_a [µm]	k_2 [µm^{-1}]	$\gamma_0 s_0$ [s^{-1}]	Φ_{post} [mol.m^{-2}.s^{-1}]	$\gamma'_0 s_0$ [s^{-1}]	Φ_{i2} [mol.m^{-2}.s^{-1}]	Φ_{d2} [mol.m^{-2}.s^{-1}]
$7.6.10^{-6}$	0.17	0.36	$1.9.10^{-15}$	$1.35.10^{-6}$	1.10^{-15}	5.10^{-6}	$5.5.10^{-6}$

Table 2: values of the parameters used in Eq. 10 and 11 for the simulation represented in Fig. 6.

Conclusions

In this paper, a model has been proposed in order to explain the shape of the oxidation curves for Zircaloy-4, during the transition and in the post-transition stage. This model involves the progressive transformation of small sections of the oxide surface, from the pre-transition stage to the post-transition stage, and it allows to describe the variations of the oxidation rate of Zircaloy-4, oxidised either in water vapour or in oxygen [13].

In both cases, the model takes into account a change in the rate-controlling step of the oxidation, from a diffusion step in pre-transition to an interface step during the post-transition stage. Although a reaction mechanism could not be proposed, this assumption is also in a good agreement with the accelerating effect of water vapour pressure observed after the transition.

References

[1] M. Tupin, M. Pijolat, F. Valdivieso, M. Soustelle, A. Frichet, P. Barberis : J. Nucl. Mat. Vol. 317 (2003), p. 130
[2] J.K. Dawson, G. Long, W.E. Seddon and J.F. White, J. Nucl. Mat. Vol. 25 (1968), p.179
[3] G.P. Sabol and S.B. Dalgoard, J. Electrochem. Soc. Vol. 122 (1975), p. 316
[4] E.A. Garcia, J. Nucl. Mat. Vol. 224 (1995) 299
[5] G.A. Eloff, C.J. Greyling and P.E. Viljoen, J. Nucl. Mat. Vol. 199 (1993), p.285
[6] C.C. Dollins and M. Jursich, J. Nucl. Mat. Vol. 113 (1983), p. 19
[7] U.R. Evans, Proceedings of the Ninety-first General Meeting at Louisville, Ky. (April 12, 1947), p. 547
[8] M. Cournil and G. Thomas, J. Chimie-Physique Vol. 74 (1977), p.545
[9] B. Cox, J. Nucl. Mat. Vol. 148 (1987), p.332
[10] Y. Ok and Y. Kim, J. Korean Nucl. Soc. Vol. 30 (1998), p. 396
[11] P. Bossis, G. Lelièvre, P. Barberis, X. Iltis, F. Lelièvre, 12th International Symposium ASTM, STP 1354 (2000), p. 918.
[12] C.H. Bamford and C.F.H. Tipper (Ed.): *Comprehensive Chemical Kinetics*, Vol. 22 (Elsevier Scientific Publishing Company, 1980)
[13] M. Tupin, Thesis, Saint-Etienne (2002)